A shark-inspired general model of tooth morphogenesis unveils developmental asymmetries in phenotype transitions

Roland Zimm, Fidji Berio, Mélanie Debiais-Thibaud, Nicolas Goudemand

PNAS RESEARCH ARTICLE | DEVELOPMENTAL BIOLOGY

A shark-inspired general model of tooth morphogenesis unveils developmental asymmetries in phenotype transitions

Roland Zimm[a,1], Fidji Berio[a,b], Mélanie Debiais-Thibaud[b], and Nicolas Goudemand[a]

Edited by Günter Wagner, Yale University, New Haven, CT; received October 5, 2022; accepted February 7, 2023

Developmental complexity stemming from the dynamic interplay between genetic and biomechanic factors canalizes the ways genotypes and phenotypes can change in evolution. As a paradigmatic system, we explore how changes in developmental factors generate typical tooth shape transitions. Since tooth development has mainly been researched in mammals, we contribute to a more general understanding by studying the development of tooth diversity in sharks. To this end, we build a general, but realistic, mathematical model of odontogenesis. We show that it reproduces key shark-specific features of tooth development as well as real tooth shape variation in small-spotted catsharks *Scyliorhinus canicula*. We validate our model by comparison with experiments in vivo. Strikingly, we observe that developmental transitions between tooth shapes tend to be highly degenerate, even for complex phenotypes. We also discover that the sets of developmental parameters involved in tooth shape transitions tend to depend asymmetrically on the direction of that transition. Together, our findings provide a valuable base for furthering our understanding of how developmental changes can lead to both adaptive phenotypic change and trait convergence in complex, phenotypically highly diverse, structures.

tooth development | mathematical modeling | phenotypic diversity | morphospace | evo-devo

Significance

Elucidating the developmental origins of phenotypic variation remains a central aim for evo-devo research. Teeth are particularly rich structures exhibiting abundant phenotypic diversity. Here, we chose an interdisciplinary approach to explore what changes in developmental factors may underlie typical transitions between shark tooth shapes within and between individuals. Using a realistic computational model, we unveil some counter-intuitive features of such transitions: high disparity of developmental mechanisms even for complex phenotypes and significant direction-dependent differences of the developmental factors involved. We hypothesize that these properties may be general to complex animal traits. Thus, our analysis contributes to explain the importance of contingency and prevalence of convergence in trait evolution.

The striking diversity of complex shapes is one of nature's key features biologists seek to understand. This plethora of different phenotypes is underpinned by a diversity of interacting developmental mechanisms, yet some developmental systems are capable of generating especially large phenotypic variation. Thus, studying such developmental systems will allow better associations between specific changes in development with the phenotypes they generate. Although modifiable developmental processes involve different kinds of heritable and nonheritable factors, this approach has traditionally been termed "genotype–phenotype mapping" (GPM) and has been applied to both general and specific developmental systems (1–6). While GPMs in specific systems facilitate a detailed developmental interpretation of variation found within organisms, populations, and related species, generalized GPMs offer an opportunity to explain patterns, trends, and biases observed across different developmental systems.

Teeth are a paradigmatic example of a specific structure displaying a vast amount of adaptive diversity, which was likely pivotal for the successful diversification of vertebrates. Besides usually varying between taxa, teeth often show conspicuous shape variation within a species or even within an individual's jaws, suggesting that there are multiple accessible ways to modify and fine-tune development locally. This has motivated researchers to explore how variation in developmental factors can be linked to certain aspects of mammalian tooth shape variation, both experimentally and in silico (1, 7, 8).

In addition, teeth and denticles are documented across most of the vertebrate phylum (9–11), offering an opportunity to link developmental and phenotypic variation to macroevolutionary trends. However, the vast majority of studies has focused on mammalian tooth development, where many relevant genetic pathways and the mechanisms of their interaction with different tissues have hence been described (12–15). Recently, research has begun unveiling features of tooth development in elasmobranchs, one of the phylogenetically most distant clades from mammals to exhibit important tooth variation (10, 16–18). Studying their dentitions might even provide a glimpse on how teeth emerged from ancestral, more general forms of ectodermal appendages, as elasmobranch integuments are covered by an array of tooth-like denticles (19).

Although many odontogenetic processes can be considered conserved between mammals and elasmobranchs (20–22), there are evident differences. Odontogenesis in mammals tends to take place much more deeply within the oral tissue than in elasmobranchs (23), where teeth form superficially and continuously, exhibiting a "conveyer-belt"–like fashion of permanent tooth replacement (16, 24). In mammals, reciprocal signaling

Author contributions: R.Z., F.B., M.D.-T., and N.G. designed research; R.Z. and F.B. performed research; R.Z. contributed new reagents/analytic tools; R.Z. and F.B. analyzed data; and R.Z., M.D.-T., and N.G. wrote the paper.

The authors declare no competing interest.

This article is a PNAS Direct Submission.

[1]To whom correspondence may be addressed. Email: zimm.roland@gmail.com.

This article contains supporting information online at http://www.pnas.org/lookup/suppl/doi:10.1073/pnas.2216959120/-/DCSupplemental.

Published April 7, 2023.

between epithelial and mesenchymal compartments of the tooth bud will lead to the formation of an epithelial signaling center termed enamel knot. Enamel knots will both promote peripheral proliferation and a local switch to differentiation which induces cusp formation. In sharks, this specialized structure has been claimed to be either absent or present in a significantly different form (18, 25). The positioning of future cusps has been suggested to be controlled by a Turing mechanism (26). In this mechanism, pro-proliferative morphogens, e.g., *Fgfs* and *Shh* (fibroblast growth factors and Sonic hedgehog) (27–29), and antiproliferative morphogens, e.g., *Bmps* bone morphogenetic proteins (30), form a signaling network giving rise to a spatially stable morphogen expression pattern, as predicted theoretically (26, 31, 32). While the mostly colocalized expression patterns of *Fgf, Shh* and *Bmp* genes in rodent tooth germs are in line with a classic Turing mechanism (33–36), expression domains of the homologous genes appear as mutually exclusive in sharks (18, 25). Surprisingly, the development of some shark skin denticles has been suggested to have more similarities with mammalian than shark oral teeth (18).

The richness of data on rodent tooth development allowed a mathematical model of mammalian odontogenesis to be built: ToothMaker (8). It has been a versatile tool to learn about the relationship between developmental and phenotypic variation in various mammalian contexts, as well as some aspects of evolution of complex traits (1, 8, 37, 38). Yet, as ToothMaker was conceived to encapsulate features of mammalian tooth development, we implemented some changes in order to properly account for odontogenesis in other clades. Thus, we built a more generalized version of this model capable of encompassing characteristics of shark tooth development, besides mammalian odontogenesis.

We used this model to understand how development can give rise to characteristic tooth shape shifts within catshark dentitions which, in addition, are reminiscent of tooth shape changes across sharks. In particular, these changes comprise different cusp numbers and relative cusp shapes, which may vary along the jaw axis (39) or between species (40). Previous work in mice suggested that it is easier to produce simple than complex teeth (41). Thus, using an in silico approach that allows us to explore a general tooth morphospace, we attempted to learn whether this observation is a general feature of tooth development and how difficult it is to evolve complex, adaptive tooth phenotypes.

Results

A Generalized Reaction-Diffusion GRN Topology Provides a Means to Reproduce Features of Shark Tooth Development. The original signaling kernel of ToothMaker consists of one molecular activator and its inhibitor, exploiting their capacity of spatially stable pattern formation via a classic activator–inhibitor-type Turing reaction–diffusion mechanism. Since in such networks, the inhibitor's expression relies on the activator's presence (31), both molecules' expressions center in the same spot, thereby not accounting for spatially exclusive expression patterns, as observed in sharks (18, 25). However, another class of reaction–diffusion mechanisms, the so-called substrate-depletion mechanisms, is characterized by out-of-phase localization of activatory and inhibitory agents (31, 42).

Thus, we changed the original signaling kernel to a three-agent signaling network capable of reproducing the characteristic spatiotemporal patterns of *Fgf, Shh*, and *Bmp*. In this network (Fig. 1*B*), S_1 (analogous to *Fgf*) activates both the S_3 (analogous to *Shh*) signal (43, 44) and the auto-stabilizing S_2 (analogous to *Bmp*) signal (19, 45–48), with S_2 (*Bmp*) acting as an inhibitor of the S_1 (*Fgf*) signal (49) and, conditionally (50), as an inhibitor of the S_3 (*Shh*) signal.

Under this model, in silico teeth showed enhanced S_3 and S_1 (*Shh* and *Fgf*) signaling in the tips of nascent cusps, while S_2 (*Bmp*) signaling was seen to localize basally to those tips, due to the negative interactions between S_2 and S_3 (cf. Fig. 1*A*). Thus, we conclude that our model is in line with the developmental features characteristic of catshark odontogenesis.

From a theoretical perspective, the implemented changes into the signaling network allowed its dynamics to shift from

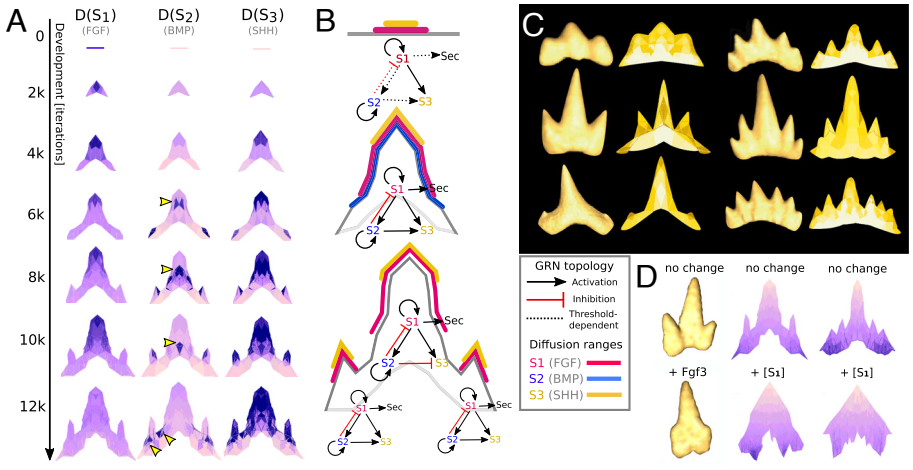

Fig. 1. The mathematical model reproduces features of shark dentitions. (*A*) Tooth development in silico. Columns show modeled tooth shapes at different developmental time points, where darker color shades represent local signaling intensity of S_1,S_2, and S_3 (*Fgf, Bmp or Shh*) expression (cf. refs. 10, 17, 18, and 25). Yellow arrowheads point to characteristic basal localization of S_2 (*Bmp*). (*B*) Signaling network dynamics of the shark tooth model. The interactions of S_1,S_2, and S_3, in analogy to *Fgf, Bmp, and Shh* (cf.refs. 10, 17, 18, and 25), and secondary activator (Sec) pathways are indicated as networks where black arrows denote activatory and red bars denote inhibitory interactions. Connections whose activity is threshold-dependent are drawn with dotted lines. The presumptive range of action of the signaling molecules is indicated by idealized colored bands above a gray epithelial–mesenchymal interface of the developing tooth bud. (*C*) In silico shark tooth shapes encompass dental diversity in *S. canicula*. Juxtaposed example pairs of CT-scanned (*Left*) and modeled (*Right*) teeth. The modeled teeth were found by random parameter screens in a generic in silico 5-cusp tooth. CT scans were taken from ref. 40. (*D*) Ectopic increase of *Fgf3* and a_1 activity simplifies tooth shapes in vivo and in silico. *Left*: CT scans of example *S. canicula* hatchling teeth without (*Upper*) and with (*Lower*) *Fgf*3-coated bead. *Middle*/*Right*: In the model, baseline S_1-activation (by the parameter a_1) is present. We increased a_1 to two-fold in a 3-cuspid and a 5-cuspid in silico tooth.

a classic activator–inhibitor system to a substrate-depletion system where S_2 can act as an activator of its substrate S_1. Since interactions between the signals are defined by parameter values, it is theoretically possible to adjust these so that classic activator–inhibitor dynamics, where signals coincide spatially, emerge again. An in-depth analysis of the network topology reveals that it shows structural features associated with relatively large Turing spaces—the proportion of parameter combinations allowing for Turing pattern emergence—possibly explaining why it was found by our morphospace exploration and why it might provide developmentally and evolutionarily robust patterning dynamics (42, 51). Since the model encompasses, by suitable parameterization, the mammalian tooth development dynamics as well, it can be considered general.

The Model Recapitulates Natural and Experimentally Induced Shape Variation. Next, we explored to which extent the model can help understand some of the natural variation of *S. canicula* dentition. In this species, tooth shapes vary both between populations, sexes, ages, and within jaws (40, 52), comprising cusp numbers between 1 and 7, symmetrical and asymmetrical teeth, as well as different cusp heights and different height ratios between neighboring cusps in multicuspid teeth (cf. *SI Appendix*, Fig. S1). Catshark cuspidity (cusp number) tends to increase from medial to distal teeth, which appears reminiscent of within-jaw cuspidity trends in other shark species and even in many mammals (21, 39, 40, 52, 53).

By exploring different combinations of the developmental model parameters, we found variants that closely resembled typical 1-cuspid, 3-cuspid, 5-cuspid, and other multicuspid teeth in *S. canicula* (Fig. 1*D*). We also found that different parameter combinations were capable of producing very similar tooth shapes.

In order to corroborate the model further, we tested if it accounts for phenotypic variation resulting from experimentally changed signaling. Although many signaling pathways are involved in tooth development, we hypothesized that *Fgfs* are particularly interesting, as interfering with *Fgf* signaling has been reported to lead to conspicuous effects in other ectodermal appendages. Ectopic *Fgfs* partially rescue cusp relief in ectodysplasin mutant mice (54) and increase proliferation in developing dental tissues in mice (55) and zebrafish (56), while ectopic *Fgf* inhibitors reduced denticle size, or prevented their formation, in the dorsal midline in sharks (57). In other ectodermal organs, the effects of ectopic *Fgf* differed (58–61), so we concluded that elucidating its effect on shark odontogenesis may be insightful.

Similar to previous studies (54, 57), we implanted beads coated with *Fgf3* into the dental laminae of *S. canicula* embryos (40). Teeth in treated laminae displayed significantly fewer cusps (averages control = 3.1, treatment = 2.3, *P*-val = 0.008), more abnormal accessory cusps (control = 0.09, treatment = 0.59, *P*-val = 0.018), and more undermineralized teeth (control = 0%, treatment = 25.9%, *P*-val = 0.01). In summary, most tooth buds treated with *Fgf3* showed underdeveloped or undeveloped accessory cusps.

To reproduce the bead experiments in silico, we ectopically increased S_1 (*Fgf*) concentration in the model in a transcription-independent manner. Ectopic increase in S_1 led to a reduction of tooth complexity, and even moderate addition of S_1 activity, such as a 2-fold increase of the parameter a_1, prevented accessory cusps from forming. We observed this for different in silico teeth with different cusp numbers (Fig. 1*D*), suggesting that the model robustly reproduces the global effect of increased *Fgf* signaling, in line with the observation in real shark tooth development.

Developmental Transitions Tend to Be Highly Degenerate. We then wanted to understand which parameter combinations have to be changed in order to transform biologically relevant phenotypes into another. Since phenotypic changes within catshark dentitions commonly involve changes in cuspidity, we attempted to transform a characteristic 3-cuspid in silico tooth into a characteristic 5-cuspid tooth shape, and vice versa. To this end, we picked a 3-cuspid and a 5-cuspid tooth from the ensemble of modeled teeth most similar to chosen real teeth of *S. canicula* (cf. *SI Appendix, Methods: Morphological Distances*). From each starting morphology, we produced a large set of random variants, which we compared to the other (target) shape. Variants were then ranked by similarity to the target (*SI Appendix*, Fig. S4). Since different combinations of developmental parameters produced similar phenotypes, we measured parameter-phenotype degeneracy (Fig. 2*B*; here defined as the parameter disparity per morphological disparity). This was done by calculating the average parameter distance (the Hamming distance, cf. *SI Appendix, Methods: Size of Phenotypic Regions*) between any two variants that were similar enough to the target shape (the "opposite" tooth shape), for different similarity rank thresholds *theta* (Fig. 2*B* and *SI Appendix*, Fig. S6). The average parameter disparity saturated quickly, approaching the global average of the entire set of variants already for similarity rank thresholds of around *theta* = 60. Representing random associations between parameters and phenotypes, we performed bootstraps of random pairs of variants as a negative control. Although degeneracy for 5-to-3 cuspid transitions tended to stay below this control, it remained largely within its 0.95 CI for 3-to-5 cuspid transitions.

In contrast, a positive control, representing a perfect correlation between parameter dissimilarity and phenotypic distance, differed substantially from the degeneracy in our ensemble data (cf. Fig. 2*B*). This suggested a high degeneracy for a complex phenotype (5-cuspid) which was supported by a comparison of degeneracies across the entire ensemble of variants (*SI Appendix*, Fig. S6). We also visualized the distribution of similar variants within the morphospace using a principal component analysis (PCA) of normalized developmental parameters. Variants with high phenotypic similarity to the target shape localized in different parts of the morphospace, without any discernible clustering (Fig. 2*A*). Using a Hotelling's T2 test, we found no difference between those clusters and the remainder of the variants in the morphospace (all *P*-values < 2e-16, except 100 best fits (*P*-value = 0.00256) and 200 best fits (*P*-value = 3.2e-7) of 3-cuspid variants against the 3-cuspid target shape). Thus, our results imply that specific associations between developmental (or genetic) parameter variations and specific phenotype transitions tend to be intrinsically difficult to establish, as many and very different combinations of parameter values led to similar phenotypic results.

Asymmetry Between Tooth Shape Transitions. The high degeneracies prevented a clear association between specific parameters and shapes. Therefore, we assessed if any parameters were mutated more often within sets of in silico variants with high similarity to the target shape. We quantified parameter enrichments both for phenotypic transitions from 3-cuspid to 5-cuspid teeth and the reverse (Fig. 3). We found that some morphogen interaction strengths mostly involving S_3 (*Shh*) signaling were changed more often than expected by

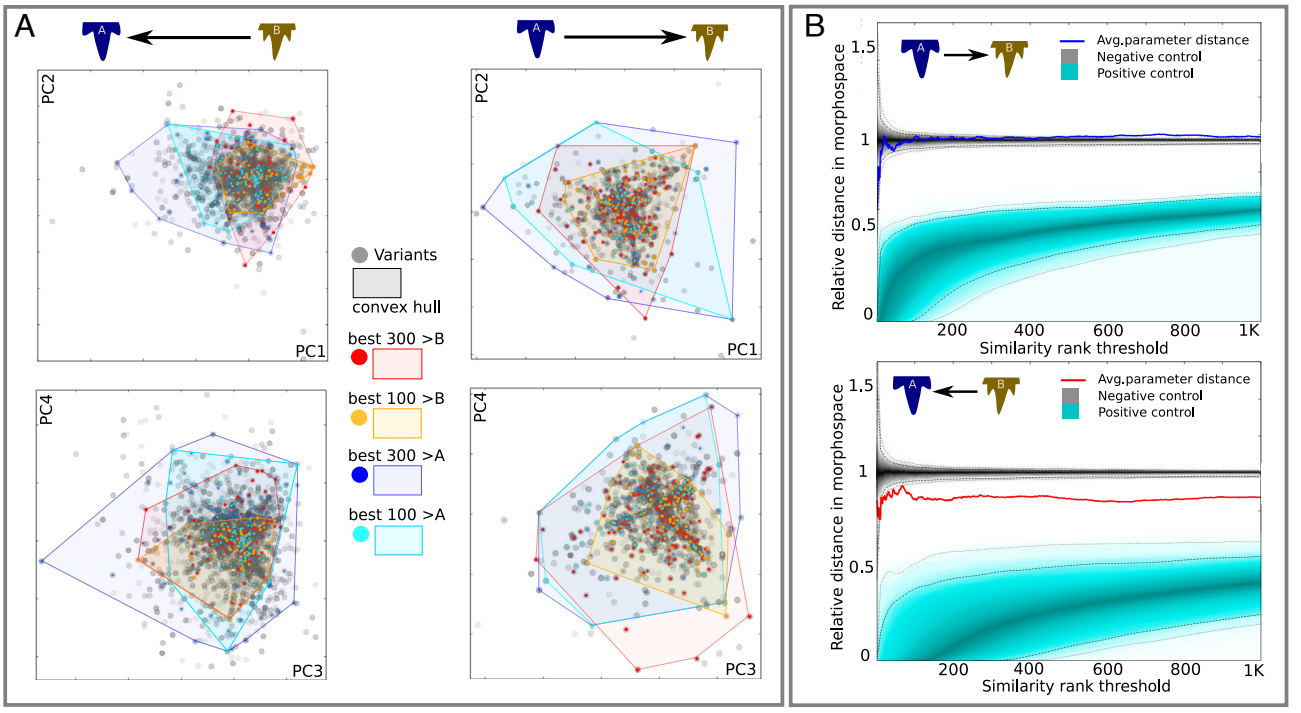

Fig. 2. The generative tooth morphospace is highly degenerate. (*A*) Principal Component Analysis of parameter changes in the generative morphospace. We show the distribution of variants between the first four PCs, for 3-to-5-cuspid transitions (N = 6,262) and vice versa (N = 3,267); colors indicate grouped similarity to target shapes (by rank threshold). Convex hulls are drawn for phenotypic regions around the target shapes. Good fit variants are distributed all over the morphospace with hulls commensurate to the entire morphospace. (*B*) Regions in the morphospace tend to be highly degenerate. Variants were ranked by phenotypic similarity to their target. Variant subsets were defined by similarity below a threshold rank. For different such thresholds, here ordered along the x-axes, the average Hamming distance between the parameter values of all variant pairs within the respective subset is associated on the y-axis (normalized for subset size and total average parameter distance for all variants). Averages are plotted in dark blue for variants of 3-cusp teeth ranked by their similarity to a target 5-cusp tooth and in red for the opposite. We performed bootstraps of 400 permutations. The resulting area is plotted in gray whose darkness represents density, with the 0.95 and 0.99 confidence intervals as dashed lines. The borders of these areas are smoothened using a Bezier algorithm. As a positive control, we also randomly picked 400 variants and ranked, for each of them, all other variants by parameter similarity to them. We then used this rank instead of the phenotypic similarity rank threshold and proceeded as described above. Results are plotted in turquoise. This way, we emulate the hypothetical case of phenotype-based distance being perfectly correlated with parameter-based distance. Since the blue and red curves are distant from the turquoise area, we conclude that this correlation is low and the overall disparity of different sets of parameters mapping to the same phenotype is high, especially for the 3-to-5 cusps transitions.

chance. This was also true for some parameters that define the mechanical properties of the tissue underlying the tooth bud (Fig. 3*A*). On the other hand, other parameters such as upstream activation, differentiation, epithelial growth, and spatial biases were changed less frequently than expected by chance. For some parameters, however, enrichment depended on the direction of the phenotypic transition (Fig. 3*A*).

To quantify direction-dependent enrichment differences, we divided, for each parameter, enrichment in the 3- to 5-cuspid variants sample by enrichment in the opposite variants sample and inverted the ratio if it was below one (Fig. 3*B*).

We found the enrichment asymmetry in our experiment to be significantly larger than in a bootstrap control (P = 0.00214); Fig. 4*A*).

To quantify this difference, we then used a sample of 200 random shapes (verifying a comparable phenotypic distance) as control target shapes and compared their parameter enrichments, individually, with the enrichments from 3-to-5 and 5-to-3 cuspid teeth. Surprisingly, the distributions between the two-way enrichment and the positive control enrichment asymmetries were not significantly different from one another (P = 0.4725), suggesting that the difference in developmental parameters between "forward" and "backward" variants is about as large as between sets of parameter changes that lead to two completely different phenotypes, for a given approximate phenotypic distance. We did not find any significant difference (P = 0.6) between the best-fit variants and random variants from the entire set, although the former tended to be slightly more asymmetric.

To make sure that this result was not a mere artifact of neutral parameter changes, we quantified the phenotypic difference that each parameter change contributed to. In total, less than 20% of mutations led to phenotypic changes that we considered insignificant, suggesting that the asymmetry we measured was not driven by a major percentage of mutations of negligible phenotypic impact (cf. *SI Appendix*, Fig. S5).

Anisotropy Differences Between Phenotypic Regions. To better understand this finding, we investigated the extent to which phenotypes were more sensitive to changes in some parameters relative to others. If a given phenotype is equally sensitive to all relative parameter changes, we would call the associated region of the parameter space isotropic, allowing for equally large parameter changes without altering the phenotype. An isotropic region of the parameter space associated with a particular phenotype would appear circular in shape (In addition, it might be reasonable to assume that most robust "wild-type" phenotypes would tend to be found at the center of such a circular region, cf. ref. 62). Otherwise, we call it anisotropic. Here, we define anisotropy as the relative difference in sensitivity to different developmental parameters (or their linear combinations) for a given phenotype. As a way to quantify

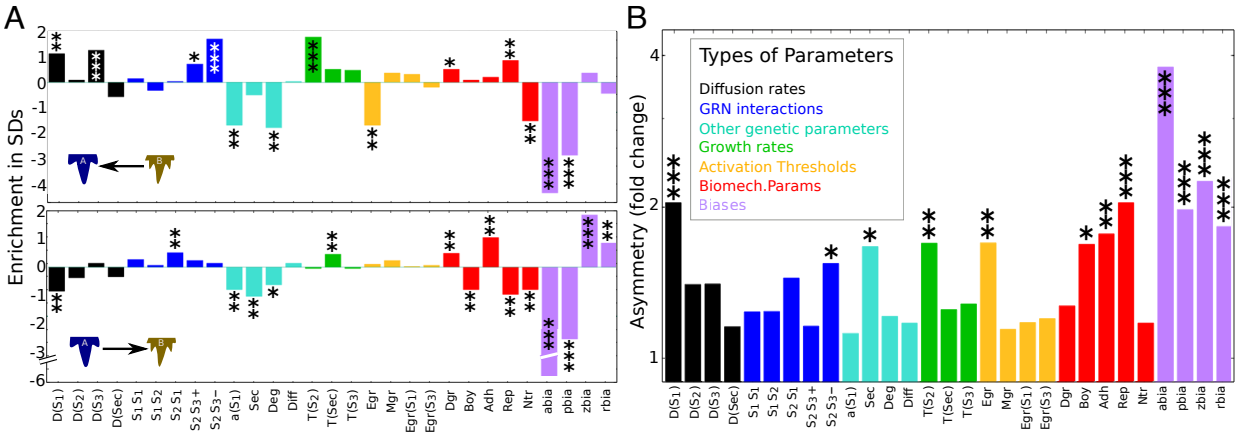

Fig. 3. Parameter enrichment and asymmetry. We isolated the 10% variants of a typical 3-cuspid in silico tooth with the lowest phenotypical distance to a typical 5-cuspid target tooth, and vice versa (cf. Fig. 2). (*A*) For either experiment, we show how often each parameter was mutated relative to what would be expected by chance, i.e., enrichments (0 represents average value expected by chance). Bar heights represent change normalized by standard deviations (SDs). (*B*) To calculate the asymmetry of enrichments, we divided, parameter-wise, the ratio between both enrichments. Ratios below one were inverted. Ratios are shown in logscale (2). Colors encode different parameter types, as shown by the *Inset*. Significance was assigned by comparison to a null-model (10^5 simulations) and is indicated by asterisks (*:$0.01 < P < 0.05$; **:$0.001 < P < 0.01$; ***:$P < 0.001$).

anisotropy, we measured parameter value differences between all pairs of variants within the same phenotypic region (defined by rank threshold). Parameter-wise ranges were then defined as absolute maxima or average differences. Then, we compared parameter ranges within the phenotypic regions around the 3- and the 5-cuspid target shapes. These calculated ranges varied substantially between the parameters (*SI Appendix*, Fig. S8), while epithelial growth rates occupied relatively large ranges, this was less so for biophysical parameters. Conspicuous differences between the two sets of best-fit variants were recorded for many developmental parameters, including epithelial growth rates, tissue adhesion, tissue rounding, diffusion rates of S_2 (*Bmp*) and S_3 (*Shh*), apical-basal biases, and mesenchymal growth rates (*SI Appendix*, Fig. S8). We then calculated the parameter-wise ratios between the parameter ranges of the two phenotypic regions. Our measurements showed substantial disparity between these ratios, indicating a large difference between the two corresponding phenotypic regions in their dependence on specific parameter variation. In every instance, the anisotropy between the two phenotypic regions proved significantly higher (Fig. 4*B* and *SI Appendix*, Fig. S8) than the respective negative controls.

Discussion

Shark Tooth Development in the Wider Context of Ectodermal Appendages. Ectodermal organs have been considered one paradigm of adaptive diversity across vertebrates (63–66). Understanding how the mechanisms of their development have evolved and how they are capable of producing a multitude of different structures and phenotypes is therefore a key question of evo-devo research (9, 19, 61, 67–73). As our study was built on a more general model of odontogenesis, it investigates developmental differences in a conserved structure between two phylogenetically distant branches of vertebrates whose last common ancestor lived more than 415 Ma ago (11, 74).

Although our proposed network of three interacting signaling pathways is still substantially simplified compared to the complexity and size of real regulatory networks, we found it sufficient to account for key developmental dynamics and observed features of odontogenesis in *S. canicula*, including spatiotemporal patterns of key morphogen pathways (10, 18). The implemented changes to the structure of the original model designed to encapsulate mammal-specific odontogenesis exemplify how developmental systems may switch their patterning modes by developmental systems drift during evolution (42, 75, 76). A recent study explained ontogenetic shifts in shark tooth cusp number using the mammal-specific version of ToothMaker (25), highlighting conserved aspects of tooth development. Here, we have showed that our generalized odontogenetic network is capable of generating specific tooth variation characteristic of within-species variation (heterodonty) in *S. canicula* (40, 77) and possibly in other species (77, 78). Besides, it is in accordance with GRNs proposed for the development of other ectodermal organs (19, 57, 79–81).

Developmental studies in ectodermal organs largely support a simplifying effect of *Fgf* on several ectodermal organs and can thus be considered in line with our observations in shark teeth (58, 59, 61). A striking difference, however, emerges when comparing the effects of ectopic *Fgf* on odontogenesis between catshark and both rodents and zebrafish, representing diverged branches within the osteichthyan clade. Although the commonalities with other ectodermal organs point to an overall high degree of conservation in the morphogenetic kernel that orchestrates patterning of ectodermal appendages, opposite effects of increased *Fgf* signaling between chondrichthyan and osteichthyan (incl. tetrapods) teeth (54–56) suggest that specific morphogen functions can diverge in a process of developmental systems drift (76) without affecting the overall developmental process or its capacity of generating phenotypic variation.

This means that morphological correspondence between two structures in divergent clades may not be a sufficient criterion to infer developmental commonalities. Thus, functionally and histologically similar structures may have evolved several times within vertebrates from a general, presumably odontode-like, ancestral appendage, due to a highly modular and plastic set of developmental mechanisms.

Specific Parameter Changes Can Be Associated with Shape Variation. The finding that specific parameters were altered significantly more often than by chance in silico (Fig. 3 and *SI Appendix*, Fig. S8) does not necessarily imply that aspects of real development corresponding to those parameters contribute critically to tooth heterodonty in shark dentitions. However, they

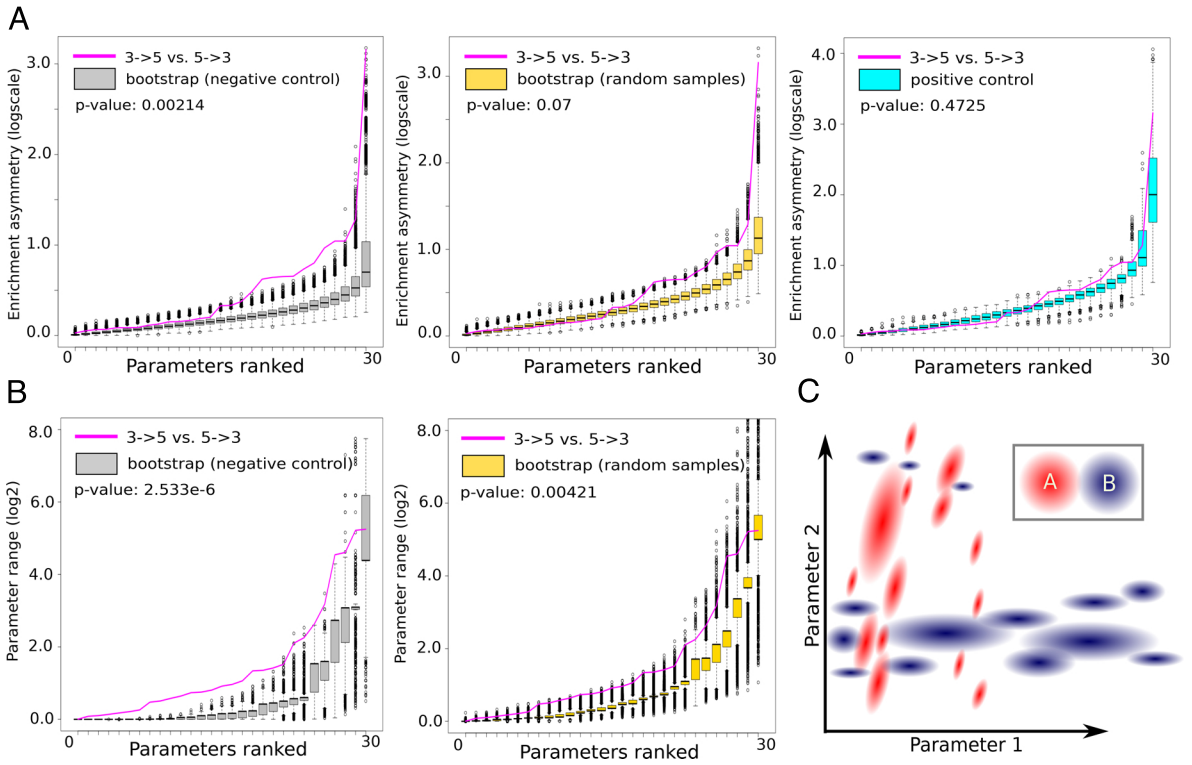

Fig. 4. Phenotypic transitions tend to be asymmetrical. (*A*) Parameter enrichment asymmetries are significant. Magenta lines represent sorted parameter-wise enrichment asymmetries. Gray boxplots display a negative control consisting of 2,000 bootstrap permutations of the same data. Turquoise boxplots represent a positive control for which different sets of variants were identified as approximately equidistant to both the 3-cusp and the 5-cusp targets. Ratios between parameter enrichments in these variants and the 3-to-5-cusp or 5-to-3-cusp best-fit variants were calculated, representing parameter enrichment differences between unrelated morphologies. Golden boxplots represent the ratios between the sets of best-fit variants and randomly chosen sets of variants; 2,000 permutations were performed. (*B*) Anisotropy: among the 100 and 200 best-fit variants, we calculated the average parameter distances between any pair of variants within those sets. This was performed for the 3-to-5-cusp variants and the reverse experiment. For each parameter, the ratio between the values from both corresponding experiments was calculated. Sorted range ratios of all parameters were plotted as a magenta line. Gray boxplots represent, as a negative control, 2,000 bootstrap permutations from the respective sets of variants. Golden boxes resulted from 2,000 bootstrap permutations based on the entire ensemble of variants. The farthest outliers are not shown. (*C*) Abstract representation of asymmetry and anisotropy of phenotypic regions. Phenotypic regions A and B are plotted as diffuse clouds of patches of the corresponding color in a reduced morphospace consisting of different combinations of values of parameter1 (p1) and parameter2 (p2). Phenotype A is more sensitive to changes in p1 than p2, while the reverse is true for phenotype B, suggesting both their phenotypic regions are anisotropic. Transiting from region B to region A will, therefore, critically depend on adjusting p1, while p2 may be altered to most values without phenotypic effects. The reverse transition, from *A* to *B*, will mostly depend on fine-tuning p2. Thus, we can expect to observe an asymmetry in the enrichments of parameter-wise changes.

represent a starting point about where to look for developmental features associated with shape variation. Diffusion rates, for instance, have been linked developmentally to the number of, and distance between, emergent cusps (15, 26), yet they did only emerge as enriched in $5 > 3$ transitions. Where diffusion ranges were changed, their values were found to be of similar magnitude (i.e., narrow parameter ranges, cf. *SI Appendix*, Fig. S8). This can be explained by a high sensitivity of reaction–diffusion dynamics to altered diffusion rates (31, 32, 51, 75, 82), which can easily disrupt the overall tooth shape, unless they are modified concordantly in both the activator and inhibitor. Thus, the more fine-tuned changes required to produce a specific 5-cuspid shape did not involve many diffusion rate modifications. Signaling interactions, however, especially those that involve S_3 (*Shh*), were found to be altered frequently (Fig. 3), suggesting that their fine-tuning might be essential for stable Turing patterns and fine-tuning cuspidities. Another study reproduced some of the effects of ectopically modified Wnt on catshark cuspidity by mainly modifying the autoactivation rate of the activator within the reaction–diffusion kernel of ToothMaker (25), adding evidence that the signaling interactions can be powerful tools to generate different cuspidities.

In mammals, a central role of tissue biomechanics has been explored with respect to the capacity of forming secondary cusps (83). In line with this, we found tissue downgrowth and adhesion, which define the specific deformations of mesenchyme and epithelium during odontogenesis, to be strongly enriched in our experiments. Conversely, other parameters like epithelial growth rate and spatial biases, some of which were even associated with heterodont seal tooth changes in another in silico study (8), did appear as depleted in our enrichment analysis. We attribute this to a high sensitivity of morphological features to changes in those parameters, leading to rather disruptive effects of their modification.

When trying to associate certain parameters with possible mechanisms that may explain heterodont variation, we have to take into consideration the likelihood that analogous features of real development can actually change within the spatial tissue context of the jaw. Thus, we might argue that differences in tissue growth might result from gradients of growth factors within the jaw (84, 85), and that changes in some biomechanic parameters might reflect different tissue thicknesses at different specific positions, making those parameters interesting candidates for explaining heterodont variation.

Morphological Transitions Are Degenerate with Respect to Developmental Mechanisms. This study shows that not only are there multiple ways to build a specific phenotype but even any substantial clustering of dominant parameter combinations can be elusive. Degeneracy was found to be high even for complex phenotypes, implying that regions of specific phenotypes within the larger morphospace tend to be vast and patchy. In other words, attributing specific and compact parts of the morphospace to specific phenotypes, and vice versa, may often reflect reality poorly.

Intriguingly, similar 5-cuspid teeth issuing from 3-cuspid teeth show even higher parameter disparity than any randomly picked pair of tooth variants. This might, ultimately, reflect that 3-cuspid teeth are morphologically simpler than 5-cuspid teeth: simpler phenotypes emerge from a larger number of parameter combinations, implying that the majority of random variants of a 3-cuspid parent will display barely changed morphologies (1, 86) that fill the parameter space densely. Conversely, almost any random modification to developments producing complex phenotypes will either lead to simpler or very different phenotypes. This could also be the chief reason why more parameters had to be adjusted to reproduce a multicuspid tooth shape than a unicuspid one in a study using ToothMaker (25), and in another study, several signaling pathways had to be fine-tuned in order to increase cuspidity in mouse molar in vitro cultures (41). Consequently, a much larger part of the successfully developed (i.e., nonfailing) variants of the 5-cuspid parent than of the 3-cuspid parent will look phenotypically similar to their target. Thus, the density and average parameter similarity will be higher in the former set, as reflected by the lower overall degeneracy. The latter, on the other hand, representing an overall rarer phenotype, will constitute dispersed islands within the morphospace, surrounded by regions of mostly simpler shapes (1, 86) (Fig. 4*C*). Although those islands might be well connected and contiguous, it is very unlikely that a random parameter exploration will uncover those spurious and reticulate connections, leading to the impression of high dispersion and degeneracy.

From an evolutionary perspective, the richness in alternative paths toward a selective phenotype might explain why certain aspects of phenotypic variation—such as the common pattern of increasing cusp numbers toward the distal part of the jaw—appear to be conserved between sharks and mammals despite substantial modifications in development (22, 39, 77, 84, 85). If various combinations of parameters can give rise to the same phenotype, it is likely that some drift in the generative factors does not crucially affect the variational aspects of the phenotypic outcome, which implies that similar structures might actually be produced in substantially different ways and that such developmental divergences might be common. This phenomenon is sometimes referred to as phenogenetic drift or developmental systems drift (87), and its occurrence in our simplified in silico model suggests that it might be an intrinsic property of developmental systems. On the other hand, the convergence of specific phenotypic traits will be a rather commonplace phenomenon too (5, 6), as disparate branches of a specific phenotypic region can be accessed from many places of the morphospace: Our study shows that we can expect the parameter disparity of such a region to approach the parameter disparity of the entire morphospace (cf. Fig. 2*A*). Then, the fact that different parts of the same phenotypic region must be adjacent to very different sets of neighboring regions also means that a specific mutation might be likely to have different phenotypic outcomes in two phenotypically conserved, but developmentally diverged, populations, thus affecting future evolution (1, 88). Such a developmental degeneracy may even facilitate the emergence of heterodonty, i.e., phenotypic variation within the same organism, as it increases the likelihood that existing patterning cues between different body parts will in some way connect to the tooth developmental program and produce the selected variation (85). In the case of *Scyliorhinus*, heterodont tooth shape transitions involving changes in cusp numbers correlate with age, sex, and jaw position (39, 52). Yet, our theoretical results suggest that the mechanisms underlying each of those transitions may be different in each instance and that we should be careful when generalizing or inferring mechanistic hypotheses even within the same organism (89). Intriguingly, since real developmental systems feature a much higher number of morphogen interactions than our model, we should expect that our observations may be even more significant in real phenotypes. As intricate developmental mechanisms involving numerous and heterogeneous developmental factors are rather commonplace in animals, this finding may, arguably, not be restricted to odontogenesis, but may be a feature of most dynamic developmental systems (90).

Previous studies, including theoretical and experimental work (1, 41, 86), have argued that there should be always more ways to reduce pattern complexity (e.g., cusp numbers) than to increase it. From a theoretical point of view (1, 86, 91), this is a consequence of the difficulty of fine-tuning several parameters required to build a complex phenotype. Yet, we showed that even in the case of higher cuspidities, the diversity of apt modifications to the morphogenetic program is large, providing a fertile playground for evolutionary drift and adaptations. Therefore, we predict that our observations would be even more salient in transitions between the very common unicuspid teeth and any other dental phenotypes.

Developmental Asymmetries Emerge from the Multidimensional Structure of Development. As one of the key results of this study, we documented a striking asymmetry between reciprocal sets of morphogenetic mechanisms. Parameter modifications leading to reciprocal phenotypic changes were found to be as different as modifications leading to completely different phenotypes. Our analysis also proposes a probable explanation of this finding: The substantial shape anisotropy of phenotypic regions. This can be better visualized in a simplified morphospace of two dimensions, whose two axes represent the possible values of two developmental parameters (represented in Fig. 4*C*). Phenotypic regions will then be represented as areas whose main axes of variation are unlikely to be parallel (or isotropic in the multidimensional case), meaning that the two phenotypes are differently robust to variation in each parameter. The more dimensions a morphospace is composed of, the more unlikely it is for phenotypic regions to be isotropic, suggesting that real phenotypic regions might prove to be even more anisotropic than in our simulations.

Yet, where does this variation in shape and orientation between phenotypic regions emerge from? We suggest that the degree of asymmetry and anisotropy between two given phenotypic regions should be related to the complexity of the respective developmental system. While relatively simple developmental systems in which few generative factors additively build a trait may allow for linear relationships between developmental parameters, this assumption cannot hold for complex developments where heterogeneous generative factors dynamically interact to produce multitrait phenotypes (92). Interacting mechanisms will unavoidably involve partially correlated change between developmental parameters, leading to complex-shaped phenotypic

regions and nongradual transitions between adjacent regions. Whether these hypotheses hold in general and which features can predict the degree of such asymmetry will be the objective of future experiments using different phenotypes and different models.

The low likelihood of reverse evolution has long been known e.g., Dollo's law (93, 94). In this study, we have conducted a systematic exploration of the developmental factors involved in typical morphological transitions in order to provide insight about why this is the case. While the results of our study suggest that morphological convergences should occur commonly, we also show that multiple trait reoccurrences within a lineage are likely to involve different underlying developmental factors. We hypothesize that this follows unavoidably from the fact that complex interactions of generative factors will create complex and differently shaped phenotypic regions, thereby crucially contributing to the central role of contingency in evolution.

Materials and Methods

Mathematical Modeling of Tooth Development. In order to simulate shark tooth development, we implemented features of shark odontogenesis into ToothMaker, in which activator–inhibitor dynamics together with tissue growth and changes in biomechanics lead to morphogenesis of the odontogenic epithelial–mesenchymal interface (8). Overall, our modification of ToothMaker is based on the assumption that most of the morphogenetic mechanisms are conserved between elasmobranchs and mammals, while developmental systems drift may have caused morphogen networks to diverge over evolutionary time (75, 76). We replaced its signaling kernel with a three-component signaling network (S_1, S_2, S_3), each, respectively, representing general features of the *Fgf*, *Bmp*, and *Shh* signaling pathways (Fig. 1*B*). The signaling factors emulating *Fgf* and *Shh* signals were defined as promoting epithelial growth. Possible upstream activation of the signaling pathways was implemented by a constant a_i. The original ToothMaker model induced signaling asymmetrically (in buccolingual direction) based on cited observations in mice, which we replaced by upstream activation of the signaling kernel from the center of the initial hexagon. Furthermore, directed pressure perpendicular to the direction of tooth eruption by the closely overlaying dental lamina was emulated. *SI Appendix, Methods: Mathematical Modelling*, for a detailed description.

Ectopic Modification of Catshark Tooth Development. We tested one model prediction by ectopically increasing Fgf signaling. This was done experimentally by implanting 100μm-sized Fgf3-coated beads into the odontogenic lamina of *S. canicula* embryos and assessing phenotypic effects. In the model, ectopic changes to the *Fgf* signal were emulated by changes to upstream activation of S_1, by modifying a_1.

Morphospace Exploration. In the first morphospace exploration phase, we created variants of in silico teeth by introducing random changes to the model parameters (*SI Appendix*, Table S1), using a logarithmic probability distribution between a parameter-specific minimum and maximum value (*SI Appendix*, Table S2). Variants were visually selected based on their similarity to general shark tooth outlines and typical distributions of signaling molecules during development. Subsequent rounds of parameter mutations were applied to zoom further into the neighborhoods of selected variants. In the second exploration phase, we produced large numbers of variants from initial in silico teeth most similar to typical 3- and 5-cuspid teeth of *S. canicula*.

Phenotype and Parameter Similarity Quantification. Shape distance between the 2D outlines of in silico variants and target shapes was quantified using normalized Euclidean distances between discrete cosine Fourier coefficients. Analogously, we measured the parameter distances between variants as normalized Euclidean distance. Parameter degeneracy was assessed as average parameter distances within sets of variants defined by a threshold phenotype distance to a target shape.

Parameter Change Enrichment and Range Anisotropies. Starting from a typical tricuspid tooth shape A, we generated the set A′ of variants and analogously used a 5-cuspid tooth shape B and its variants as the set B′ of shapes. Each variant set was sorted by similarity to a target shape: for set A′, the target shape was shape B, and vice versa. This was done to emulate shape transformations reminiscent of real toothrows in catsharks. Subsets were then delimited by a threshold similarity rank. This allowed us to compare the frequency of parameter changes between A and A′ and B and B′. Parameter-wise ratios between total counts of parameter changes in the two conditions were calculated (i.e., specific enrichments). Enrichments across all parameters were then ranked, quantifying the global parameter enrichment asymmetry. Parameter ranges were measured as the normalized distance between the highest and lowest value of the respective parameter in an entire set of variants. In analogy to enrichment asymmetries, we quantified global parameter range anisotropies by ranking parameter-wise ranges and comparison to a negative control (by bootstrap). Results were statistically assessed via Kolmogorov–Smirnoff tests.

SI datasets. Detailed methods and additional tables and figures are provided in *SI Appendix*. In addition, the code for the tooth model alongside files required for its execution and visualization is available under: https://github.com/RolandZimm/silicoshark/releases/tag/v2.0. The outlines of the 3-cuspid and 5-cuspid target shapes are provided, too. For further information, please contact the lead author.

Data, Materials, and Software Availability. All the data necessary to replicate our results alongside software and morphological data are already available in the manuscript, its supplementary material, and at an open repository: https://github.com/RolandZimm/silicoshark/releases/tag/v2.0 (546043138) (95).

ACKNOWLEDGMENTS. This study has been funded by a Deutsche Forschungsgesellschaft research fellowship (ZI1809/1-1:1, Proj.432922638) to R.Z. and a French ANR grant (PLASTICiTEETH) to N.G. We thank Cyril Charles, Jukka Jernvall, and an anonymous reviewer for helpful feedback on the manuscript. We acknowledge the MRI platform member of the national infrastructure France-BioImaging supported by the French National Research Agency (ANR-10-INBS-04, "Investments for the future"), the labex CEMEB (ANR-10-LABX-0004), and NUMEV (ANR-10-LABX-0020) and thank Sylvie Agret and Renaud Lebrun for their help with microCT imaging.

Author affiliations: [a]Institut de Génomique Fonctionnelle de Lyon, Ecole Normale Supérieure de Lyon, Université Claude Bernard Lyon 1, CNRS UMR 5242, Lyon Cedex 07 69364, France; and [b]Institut des Sciences de l'Evolution de Montpellier, University of Montpellier, CNRS, Institut de la Recherche pour le Développement, Montpellier 34095, France

1. I. Salazar-Ciudad, M. Marin-Riera, Adaptive dynamics under development-based genotype-phenotype maps. *Nature* **497**, 361–364 (2013).
2. G. P. Wagner, J. Zhang, The pleiotropic structure of the genotype-phenotype map: The evolvability of complex organisms. *Nat. Rev. Genet.* **12**, 204–213 (2011).
3. S. F. Greenbury, I. G. Johnston, A. A. Louis, S. E. Ahnert, A tractable genotype–phenotype map modelling the self-assembly of protein quaternary structure. *J. R. Soc. Interface* **11**, 20140249 (2014).
4. C. F. Arias, P. Catalán, S. Manrubia, J. A. Cuesta, toyLIFE: A computational framework to study the multi-level organization of the genotype-phenotype map. *Sci. Rep.* **4**, 1–19 (2014).
5. S. Manrubia *et al.*, From genotypes to organisms: State-of-the-art and perspectives of a cornerstone in evolutionary dynamics. *Phys. Life Rev.* **38**, 55–106 (2021).
6. A. A. Louis, Contingency, convergence and hyper-astronomical numbers in biological evolution. *Stud. History Philos. Biol. Biomed. Sci.* **58**, 107–116 (2016).
7. E. Harjunmaa *et al.*, Replaying evolutionary transitions from the dental fossil record. *Nature* **512**, 44–48 (2014).
8. I. Salazar-Ciudad, J. Jernvall, A computational model of teeth and the developmental origins of morphological variation. *Nature* **464**, 583 (2010).
9. A. Huysseune, J. Y. Sire, Evolution of patterns and processes in teeth and tooth-related tissues in non-mammalian vertebrates. *Euro. J. Oral Sci.* **106**, 437–481 (2014).
10. L. J. Rasch *et al.*, An ancient dental gene set governs development and continuous regeneration of teeth in sharks. *Dev. Biol.* **415**, 347–370 (2016).
11. P. C. J. Donoghue, M. Rücklin, The ins and outs of the evolutionary origin of teeth. *Evol. Dev.* **18**, 19–30 (2016).

12. I. Thesleff, The genetic basis of tooth development and dental defects. *Am. J. Med. Genet. Part A* **140A**, 2530–2535 (2006).
13. A. Balic, I. Thesleff, Tissue interactions regulating tooth development and renewal. *Curr. Topics Dev. Biol.* **115**, 157–186 (2015).
14. M. Tummers, I. Thesleff, The importance of signal pathway modulation in all aspects of tooth development. *J. Exp. Zool. (Mol. Dev. Evol.)* **312B**, 309–319 (2009).
15. J. Jernvall, I. Thesleff, Reiterative signaling and patterning during mammalian tooth morphogenesis. *Mech. Dev.* **92**, 19–29 (2000).
16. G. J. Fraser, A. Standing, C. Underwood, A. P. Thiery, The dental lamina: An essential structure for perpetual tooth regeneration in sharks. *Integr. Comp. Biol.* **60**, 644–655 (2020).
17. M. Debiais-Thibaud *et al*., The homology of odontodes in gnathostomes: insights from Dlx gene expression in the dogfish *Scyliorhinus canicula*. *BMC Evol. Biol.* **11**, 307 (2011).
18. M. Debiais-Thibaud *et al*., Tooth and scale morphogenesis in shark: An alternative process to the mammalian enamel knot system. *BMC Evol. Biol.* **15**, 1–17 (2015).
19. R. L. Cooper, K. J. Martin, L. J. Rasch, G. J. Fraser, Developing an ancient epithelial appendage: FGF signalling regulates early tail denticle formation in sharks. *Evol. Dev.* **8**, 1–19 (2017).
20. T. Örvig, Phylogeny of tooth tissues: Evolution of some calcified tissues in early vertebrates. *Struct. Chem. Organ. Teeth, Vol.1, A.E.W.Miles (Ed.) Academic* **1**, 45–110 (1967).
21. W. E. Reif, "Evolution of dermal skeleton and dentition in vertebrates" in *Evolutionary Biology*, M. K. Hecht, B. Wallace, G. T. Prance, Eds. (Springer, Boston, MA, 1982). https://doi.org/10.1007/978-1-4615-6968-8_7.
22. F. Berio, M. Debiais-Thibaud, Evolutionary developmental genetics of teeth and odontodes in jawed vertebrates: A perspective from the study of elasmobranchs. *J. Fish Biol.* **98**, 906–918 (2019).
23. A. S. Tucker, G. J. Fraser, Evolution and developmental diversity of tooth regeneration. *Semin. Cell Dev. Biol.* **25–26**, 71–80 (2014).
24. V. K. Märkel, L. Laubier, Zum Zahnerzatz bei Elasmobranchiern. *Zool. Beitraege* **15**, 41–44 (1969).
25. A. P. Thiery, A. S. Standing, R. L. Cooper, G. J. Fraser, An epithelial signalling centre in sharks supports homology of tooth morphogenesis in vertebrates. *eLife* **11**, e73173 (2022).
26. I. Salazar-Ciudad, J. Jernvall, A gene network model accounting for development and evolution of mammalian teeth. *Proc. Natl. Acad. Sci. U.S.A.* **99**, 8116–8120 (2002).
27. P. Kettunen, I. Karavanova, I. Thesleff, Responsiveness of developing dental tissues to fibroblast growth factors: Expression of splicing alternatives of FGFR1, -2, -3, and of FGFR4; and stimulation of cell proliferation by FGF-2, -4, -8, and -9. *Dev. Genet.* **22**, 374–385 (1998).
28. A. Gritli-Linde *et al*., Shh signaling within the dental epithelium is necessary for cell proliferation, growth and polarization. *Development* **129**, 5323–5337 (2002).
29. H. R. Dassule, P. Lewis, M. Bei, R. Maas, A. P. McMahon, Sonic hedgehog regulates growth and morphogenesis of the tooth. *Development* **127**, 4775–4785 (2000).
30. J. Jernvall, T. Åberg, P. Kettunen, S. Keränen, I. Thesleff, The life history of an embryonic signaling center: BMP-4 induces p21 and is associated with apoptosis in the mouse tooth enamel knot. *Development* **121**, 161–169 (1998).
31. A. Gierer, H. Meinhardt, A theory of biological pattern formation. *Kybernetik* **12**, 30–39 (1972).
32. S. Kondo, T. Miura, Reaction-diffusion model as a framework for understanding biological pattern formation. *Science* **329**, 1616–1620 (2010).
33. A. Vaahtokari, T. Åberg, J. Jernvall, S. Keränen, I. Thesleff, The enamel knot as a signaling center in the developing mouse tooth. *Mech. Dev.* **54**, 39–43 (1996).
34. I. Miletich *et al*., Developmental stalling and organ-autonomous regulation of morphogenesis. *Proc. Natl. Acad. Sci. U.S.A.* **108**, 19270–19275 (2011).
35. L. Zhang, F. Hua, G. Yuan, Y. D. Zhang, Z. Chen, Sonic hedgehog signalling is critical for cytodifferentiation and cusp formation in developing mouse molars. *J. Mol. Histol.* **39**, 87–94 (2008).
36. M. Seppala, G. J. Fraser, A. A. Birjandi, G. M. Xavier, M. T. Cobourne, Sonic Hedgehog signaling and development of the dentition. *J. Dev. Biol.* **5**, 6 (2017).
37. L. Milocco, I. Salazar-Ciudad, Is evolution predictable? Quantitative genetics under complex genotype-phenotype maps. *Evolution* **74**, 230–244 (1974).
38. E. Renvoisé *et al*., Mechanical constraint from growing jaw facilitates mammalian dental diversity. *Proc. Natl. Acad. Sci. U.S.A.* **114**, 9403–9408 (2017).
39. F. Berio, A. Evin, N. Goudemand, M. Debiais-Thibaud, The intraspecific diversity of tooth morphology in the large-spotted catshark *Scyliorhinus stellaris*: Insights into the ontogenetic cues driving sexual dimorphism. *J. Anatomy* **237**, 960–978 (2020).
40. Berio F, Multiscale variation of 3D tooth forms in selachians and developmental and evolutionary inferences: Odyssey of a scyliorhinid tooth. Populations and Evolution [q-bio.PE]. Université de Lyon (2021).
41. E. Harjunmaa *et al*., On the difficulty of increasing dental complexity. *Nature* **483**, 324–327 (2012).
42. X. Diego, L. Marcon, P. Müller, J. Sharpe, Key features of turing systems are determined purely by network topology. *Phys. Rev. X* **8**, 021071 (2018).
43. A. S. Tucker, P. T. Sharpe, Molecular genetics of tooth morphogenesis and patterning: The right shape in the right place. *J. Dental Res.* **78**, 826–834 (1999).
44. K. Kratochwil, J. Galceran, S. Tontsch, W. Roth, R. Grosschedl, FGF4, a direct target of LEF1 and Wnt signaling, can rescue the arrest of tooth organogenesis in Lef1(-/-) mice. *Genes Dev.* **16**, 3173–3185 (2002).
45. C. L. Beites *et al*., Follistatin modulates a BMP autoregulatory loop to control the size and patterning of sensory domains in the developing tongue. *Development* **136**, 2187–2197 (2009).
46. J. Li, C. Parada, Y. Chai, Cellular and molecular mechanisms of tooth root development. *Development* **144**, 374–384 (2017).
47. H. Peters, R. Balling, Teeth: Where and how to make them. *Trends Genet.* **15**, 59–65 (1999).
48. Y. Chen, M. Bei, I. Woo, I. Satokata, R. Maas, Msx1 controls inductive signaling in mammalian tooth morphogenesis. *Development* **122**, 449–456 (1996).
49. A. Neubüser, H. Peters, R. Balling, G. R. Martin, Antagonistic interactions between FGF and BMP signaling pathways: A mechanism for positioning the sites of tooth formation. *Cell* **90**, 247–255 (1997).
50. Y. Zhang *et al*., A new function of BMP4: Dual role for BMP4 in regulation of Sonic hedgehog expression in the mouse tooth germ. *Development* **7**, 1431–1443 (2000).
51. A. N. Landge, B. M. Jordan, X. Diego, P. Müller, Pattern formation mechanisms of self-organizing reaction-diffusion systems. *Dev. Biol.* **460**, 2–11 (2020).
52. F. Berio, Y. Bayle, D. Baum, N. Goudemand, M. Debiais-Thibaud, Hide and seek shark teeth in Random Forests: Machine learning applied to *Scyliorhinus canicula* populations. *PeerJ* **10**, e13575 (2022).
53. K. R. Selig, W. Khalid, M. T. Silcox, Mammalian molar complexity follows simple, predictable patterns. *Proc. Natl. Acad. Sci. U.S.A.* **118**, e2008850118 (2021).
54. J. Pispa *et al*., Cusp patterning defect in tabby mouse teeth and its partial rescue by FGF. *Dev. Biol.* **216**, 521–534 (1999).
55. J. Jernvall, P. Kettunen, I. Karavanova, L. B. Martin, I. Thesleff, Evidence for the role of the enamel knot as a control center in mammalian tooth cusp formation: Non-dividing cells express growth stimulating Fgf-4 gene. *Int. J. Dev. Biol.* **38**, 463–469 (1994).
56. W. R. Jackman *et al*., Manipulation of *Fgf* and *Bmp* signaling in teleost fishes suggests potential pathways for the evolutionary origin of multicuspid teeth. *Evol. Dev.* **15**, 107–118 (2013).
57. R. L. Cooper *et al*., An ancient Turing-like patterning mechanism regulates skin denticle development in sharks. *Sci. Adv.* **4**, eaau5484 (2018).
58. J. D. Glover *et al*., Hierarchical patterning modes orchestrate hair follicle morphogenesis. *PLoS Biol.* **15**, e2002117 (2017).
59. C. M. Lin *et al*., Spots and stripes: Pleomorphic patterning of stem cells via p-ERK-dependent cell chemotaxis shown by feather morphogenesis and mathematical simulation. *Dev. Biol.* **334**, 369–382 (2009).
60. T. X. Jiang, H. S. Jung, R. B. Widelitz, C. M. Chuong, Self-organization of periodic patterns by dissociated feather mesenchymal cells and the regulation of size, number and spacing of primordia. *Development* **126**, 4997–5009 (1999).
61. J. E. Moustakas-Verho *et al*., The origin and loss of periodic patterning in the turtle shell. *Development* **141**, 3033–3039 (2014).
62. E. Bornberger-Bauer, H. S. Chan, Modeling evolutionary landscapes: Mutational stability, topology, and superfunnels in sequence space. *Proc. Natl. Acad. Sci. U.S.A.* **96**, 10689–10694 (1999).
63. P. T. Sharpe, Fish scale development: Hair today, teeth and scales yesterday? *Curr. Biol.* **11**, R751–R752 (2001).
64. D. Dhouailly *et al*., Getting to the root of scales, feather and hair: As deep as odontodes? *Exp. Dermatol.* **28**, 503–508 (2017).
65. A. Sadier, L. Viriot, S. Pantalacci, V. Laudet, The ectodysplasin pathway: From diseases to adaptations. *Trends Genet.* **30**, 24–31 (2014).
66. P. Wu *et al*., Evo-Devo of amniote integuments and appendages. *Int. J. Dev. Biol.* **48**, 249–270 (2004).
67. L. C. Biggs, M. L. Mikkola, Early inductive events in ectodermal appendage morphogenesis. *Semin. Cell Dev. Biol.* **25–26**, 11–21 (2014).
68. C. M. Chuong, R. Chondankar, R. B. Widelitz, T. X. Jiang, Evo-Devo of feathers and scales: Building complex epithelial appendages. *Curr. Opin. Genet. Dev.* **10**, 449–456 (2000).
69. C. M. Chuong, C. Y. Yeh, T. X. Jiang, R. B. Widelitz, Modul-based complexity formation: Periodic patterning in feathers and hairs. *WIREs Dev. Biol.* **2**, 97–112 (2013).
70. N. Di-Poï, M. C. Milinkovitch, The anatomical placode in reptile scale morphogenesis indicates shared ancestry among skin appendages in amniotes. *Sci. Adv.* **2**, p.e1600708 (2016).
71. J. Pispa, I. Thesleff, Mechanisms of ectodermal organogenesis. *Dev. Biol.* **262**, 195–205 (2003).
72. R. B. Widelitz, J. M. Veltmaat, J. A. Mayer, J. Foleym, C. M. Chuong, Mammary glands and feathers: Comparing two skin appendages which help define novel classes during vertebrate evolution. *Semin. Cell Dev. Biol.* **18**, 255–266 (2007).
73. R. Zimm, On the development of the turtle scute pattern and the origins of its variation. Dissertationes Scholae Doctoralis ad Sanitatem Investigandam Universitatis Helsinkiensis - URN:ISSN:2342-317X **21** (2019).
74. M. Benton, P. C. J. Donoghue, R. J. Asher, "Calibrating and constraining molecular clocks" in *The Timetree of Life*, S. B. Hedges, Eds. (Oxford University Press, 2009), pp. 35–86.
75. J. Cotterell, J. Sharpe, An atlas of gene regulatory networks reveals multiple three-gene mechanisms for interpreting morphogen gradients. *Mol. Syst. Biol.* **6**, 424 (2010).
76. J. Jaeger, M. Laubichler, W. Callebaut, The comet cometh: Evolving developmental systems. *Biol. Theory* **10**, 36–49 (2015).
77. J. Herman, M. Hovestadt-Euler, D. C. Hovestadt, "Part A : Selachii. No. 2b : Order: Carcharhiniformes - Family: Scyliorhinidae" in *Contributions to the Study of the Comparative Morphology of Teeth and Other Relevant Ichthyodorulites in Living Supraspecific Taxa of Chondrichthyan Fishes*, M. Stehmann, Ed. (1990), vol. 60, pp. 81–210.
78. K. D. A. Soares, M. R. D. Carvalho, The catshark genus *Scyliorhinus* (Chondrichthyes: Carcharhiniformes: Scyliorhinidae): Taxonomy, morphology and distribution. *Zootaxa* **4601**, 1–147 (2019).
79. T. Jiang *et al*., Integument pattern formation involves genetic and epigenetic controls: Feather arrays simulated by digital hormone models. *Int. J. Dev. Biol.* **48**, 117–135 (2004).
80. M. P. Harris, J. F. Fallon, R. O. Prum, Shh-Bmp2 signaling module and the evolutionary origin and diversification of feathers. *J. Exp. Zool. (Mol. Dev. Evol.)* **294**, 160–176 (2002).
81. H. S. Jung *et al*., Local inhibitory action of bmps and their relationships with activators in feather formation: Implications for periodic patterning. *Dev. Biol.* **196**, 11–23 (1998).
82. J. D. Murray, Parameter space for turing instability in reaction diffusion mechanisms: A comparison of models. *J. Theor. Biol.* **98**, 143–163 (1982).
83. M. Marin-Riera, J. E. Moustakas-Verho, Y. Savriama, J. Jernvall, I. Salazar-Ciudad, Differential tissue growth and cell adhesion alone drive early tooth morphogenesis: An ex vivo and in silico study. *PLOS Comput. Biol.* **14**, e1005981 (2018).
84. P. M. Butler, Dental merism and tooth development. *J. Dental Res.* **46**, 845–850 (1967).
85. T. A. Mitsiadis, M. M. Smith, How do genes make teeth to order through development? *J. pf Exp. Zool. (Mol. Dev. Evol.)* **306B**, 77–182 (2006).
86. P. F. Hagolani, R. Zimm, R. Vroomans, I. Salazar-Ciudad, On the evolution and development of morphological complexity: A view from gene regulatory networks. *PLOS Comput. Biol.* **17**, e1008570 (2021).
87. K. M. Weiss, S. M. Fullerton, Phenogenetic drift and the evolution of genotype-phenotype relationships. *Theor. Popul. Biol.* **57**, 187–195 (2000).
88. A. Wagner, Robustness and evolvability: A paradox resolved. *Proc. R. Soc. B* **275**, 91–100 (2008).
89. M. Sémon *et al*., Comparison of developmental genome expression in rodent molars reveals extensive developmental system drift. bioRxiv [Preprint] (2020). 10.1101/2020.04.22.043422 (Accessed 15 September 2022).
90. I. Salazar-Ciudad, J. Jernvall, How different types of pattern formation mechanisms affect the evolution of form and development. *Evol. Dev.* **6**, 6–16 (2004).
91. P. F. Hagolani, R. Zimm, M. Marin-Riera, I. Salazar-Ciudad, Cell signalling stabilizes morphogenesis against noise. *Development* **146**, dev179309 (2019).

92. I. Salazar-Ciudad, J. Jernvall, S. Newman, Mechanisms of pattern formation in development and evolution. *Development* **130**, 2027–2037 (2003).
93. L. Dollo, Dollo on Dollo's law: Irreversibility and the status of evolutionary laws. *Bull. Soc. Belge Geol. Paleontol. Hydrol.* **7**, 164–166 (1893).
94. S. J. Gould, Dollo on Dollo's law: Irreversibility and the status of evolutionary laws. *J. History Biol.* **3**, 189–212 (1970).
95. R. Zimm, silicoshark. Github. https://github.com/RolandZimm/silicoshark/releases/tag/v2.0. Deposited 29 November 2022.